STRESSES IN YTTERBIUM SILICATE MULTILAYER ENVIRONMENTAL BARRIER COATINGS

F. Stolzenburg
Department of Materials Science and Engineering, Northwestern University, Evanston, IL 60208

J. Almer
Advanced Photon Source, Argonne National Laboratory, Argonne, IL 60439

K.N. Lee
Materials Process and Repair Technologies, Rolls-Royce Corporation, Indianapolis, IN 46241

B.J. Harder
Durability and Protective Coatings Branch, NASA Glenn Research Center, Cleveland, OH 44315

K.T. Faber
Northwestern University, Department of Materials Science and Engineering, Evanston, IL 60208

The internal stresses of plasma-sprayed multilayer ytterbium disilicate environmental barrier coatings were measured using microfocused high-energy X-rays in a transmission geometry. Stresses were measured for as-sprayed and *ex-situ* heat-treated ytterbium disilicate topcoats at room temperature and during *in-situ* heating and cooling experiments. *In-situ* loading experiments were also performed on the topcoat in order to establish its elastic constants. The ytterbium disilicate was found to have a relatively low coefficient of thermal expansion resulting in compressive stresses of approximately 100 MPa throughout the topcoat. *In-situ* heating experiments revealed a statistically significant stress relaxation in the ytterbium disilicate topcoat upon thermal cycling to temperatures above 1300°C, indicating the onset of stress relaxation but no cracks were observed in SEM micrographs. The stress states were also modeled using a numerical solution; measured stresses were found to be very close to the predicted stresses in ytterbium dilisicate topcoats, while the experimentally determined stresses in the intermediate layers were of much smaller magnitude than the calculated stresses.

I. INTRODUCTION

Due to their excellent high temperature properties, low density, and good thermo-mechanical stability, silicon-based ceramics (i.e., SiC, Si_3N_4) are one of the most promising material systems for high temperature structural applications in gas turbine engines (Jacobson, 1993; Lee, 2000a). However, a passivating SiO_2 surface layer that naturally forms on SiC and Si_3N_4 reacts with water vapor present in combustion environments. The resulting hydroxide layer volatilizes, leading to component recession (Opila, 1999; Opila et al. 1999). Environmental barrier coatings (EBCs) have been identified as a method of protection from these harsh turbine environments. Desirable properties for EBCs include good thermal and phase stability, low volatility in engine environments, and a coefficient of thermal expansion (CTE) that matches the underlying layers. Residual stresses induced by differences in CTEs between layers are the most common cause for cracking or spallation in EBCs (Evans and Hutchinson, 1984; Thouless, 1991; Lee, 2000b). Through-thickness cracks allow for water vapor to diffuse to the component, and can thus lead to premature component failure.

The most studied EBC system to date has been a three-layer coating system consisting of a silicon bond coat, an intermediate layer of mullite ($3Al_2O_3 \cdot 2SiO_2$) , and a top layer of BSAS (1-x)BaO-xSrO-Al_2O_3-$2SiO_2$, where x varies between 0 and 1 (Lee et al., 2003). The intermediate mullite layer is needed to prevent the topcoat from reacting with the Si or the substrate, while the BSAS is the active environmental barrier layer (Lee, 2000a; Lee, et al. 2003). These coating systems have proven to be very long-lasting, but on exposure to amorphous calcium magnesium aluminosilicate deposits ingested into turbines, the molten glass reacts with the topcoat and causes degradation and cracking. BSAS has also been found to react with the underlying mullite layers at high temperatures, limiting its use as a topcoat to operating temperatures below ~1300ºC (Lee et al., 2003; Lee et al., 2005). Another durability issue is cracking induced by CTE mismatches between the layers of the coating system, particularly the topcoat and the mullite (Harder et al., 2009a).

New EBC topcoat materials are needed to allow higher operating temperatures and greater efficiencies. One group of candidate materials is the family of rare-earth silicates. Studies of their thermal stability and feasibility for coating applications identified ytterbium disilicate ($Yb_2Si_2O_7$) as a promising alternative for operating temperatures up to 1500°C (Lee et al., 2005). Figure 1 shows the thermomechanical stability of hot-pressed $Yb_2Si_2O_7$ and BSAS at 1500° C in flowing 50% H_2O-balance O_2. It shows that $Yb_2Si_2O_7$has a

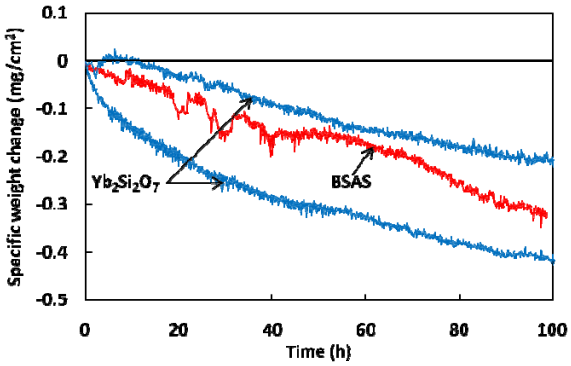

Figure 1. Volatility of hot-pressed BSAS and $Yb_2Si_2O_7$ exposed to 50% H_2O-balance O_2 flowing at 4.4 cm/s at 1500°C and 1 atm total pressure. Data adapted from Lee, 2005.

volatility comparable to that of BSAS.

The goal of this study is to use high-energy X-ray diffraction (XRD) to study the microstructure of EBCs with $Yb_2Si_2O_7$ topcoats and their resultant internal stress distributions through the multilayers. The materials used consist of a melt-infiltrated SiC/SiC ceramic-matrix composite substrate, a silicon bond layer, a mullite ($3Al_2O_3 \cdot 2SiO_2$) diffusion layer, and the $Yb_2Si_2O_7$topcoat. Stresses are reported in all layers of EBC systems both at room temperature and during heating and cooling. Comparing the measured stress distributions with numerical predictions and microscopic observations via scanning electron microscopy (SEM) allows for identification of cracks and other defects and their influence on the stresses. In order to study the evolution of stresses as these materials are used in service both as-sprayed as well as heat-treated specimen were tested. Additional *in-situ* heating experiments of samples were performed, allowing for the observation of changes in stress with heating and cooling. The mechanical properties of this new topcoat material (elastic modulus, Poisson's ratio, CTE) are not well established and were determined as part of this study via *in-situ* loading experiments. Knowing the stresses in these systems offers important insight into the feasibility of these materials as next-generation EBCs.

II. EXPERIMENTAL PROCEDURE

(a) PROCESSING

Multilayer EBCs were deposited via atmospheric plasma spray onto melt-infiltrated SiC/SiC ceramic matrix composites substrate at NASA Glenn Research Center. Details of the plasma spraying are discussed in previous publications (Lee et al., 1995; Faber et al., 2007). The EBC system consists of a 300-μm $Yb_2Si_2O_7$ topcoat and a 60-μm mullite reaction barrier layer, both sprayed onto a substrate heated to 1200°C. A 60-μm silicon layer, sprayed onto an unheated substrate, was used to improve bonding between the active EBC layers and the substrate. The full system will be referred to as a $Yb_2Si_2O_7$/Mullite/Si/(SiC/SiC) multilayer EBC. The coating was deposited onto a 12 x 6 x 3 mm^3 melt-infiltrated SiC/SiC composite coupon. Bulk $Yb_2Si_2O_7$ samples for determination of X-ray elastic constants were plasma-sprayed onto unheated graphite substrates which were subsequently removed via oxidation of the substrate at 800°C .

Samples for transmission X-ray measurements were cut into 7 mm wide, 1.5 mm thick sections. One sample was measured in the as-sprayed state, one sample was heat treated for 20h at 1300°C in flowing air and one sample was heat treated in flowing air at 1300°C for 100h. Heat treatments at higher temperatures were not possible because exposed silicon and SiC/SiC layers would oxidize during the heat treatment. Bulk $Yb_2Si_2O_7$ for the *in-situ* loading experiments was heat treated at 1100°C for 4h to obtain crystallinity similar to the as-sprayed EBC layer. Samples were machined into parallelepipeds measuring 8 x 3 x 1 mm^3.

(b) STRAIN MEASUREMENTS AND STRESS DETERMINATION

X-ray diffraction (XRD) was performed at beamline 1-ID at the Advanced Photon Source at Argonne National Lab. The high energies (70 keV) and high flux allow for the diffraction to be performed in a transmission geometry. The beam was produced using a Laue monochromator and vertically focusing Si refractive lenses. An amorphous silicon detector (General Electric Angio), placed approximately 1.2 m away from the sample, was used to collect the resulting Debye rings. Diffraction patterns from a ceria (CeO_2) standard were used to establish the sample-detector distance and other relevant parameters, such as the center point of the Debye rings and the detector tilt.

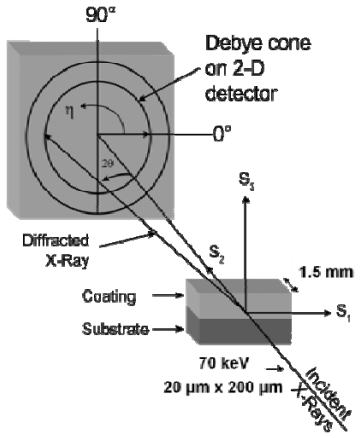

Figure 2. Schematic of the experimental set-up. Reproduced from Harder et al., 2009a.

For the measurements on the EBCs, a beam size of 200 x 20 μm^2 was used. Ten measurements were taken horizontally to achieve a diffracted volume of at least 80 μm^3. The samples were translated 20 µm vertically with respect to the beam for each measurement from the topcoat surface to a depth of 1.5 mm into the substrate for the room temperature samples and 0.5 mm for the *in-situ* heated samples. This allowed for stresses to be determined continuously as a function of depth throughout the entire coating. The total error for each measurement was comprised of statistical peak fitting errors and standard errors from the biaxial fit of lattice parameter versus azimuth.

The methodology used to calculate strains and stresses from the Debye ring patterns was identical to that used in previous experiments (Almer et al., 2003; Faber et al., 2007; Weyant et al., 2005; Weyant et al., 2006; Harder et al., 2009a; Harder et al., 2009b). Beam sizes were chosen such that enough grains were contained within the diffracted volume to yield continuous Debye ring patterns. Each ring in the Debye pattern corresponds to a specific crystallographic direction while the azimuthal angle (η) depends on the orientation of the set of planes relative to the sample. If stresses are present, the Debye rings distorts into ellipses (Figure 3). The relationship between strain in a specific azimuthal direction and deformation of the rings is described by:

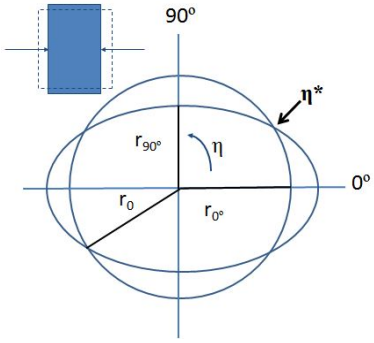

Figure 3. Compressive loading of a sample (inset) and resulting deformation of a Debye ring.

$$\varepsilon_\eta = \frac{r_0 - r_\eta}{r_0} = \frac{d_\eta - d_0}{d_0},$$

where r_0 and d_0 are the ring radius and interplanar spacing of the strain-free sample, respectively (Noyan and Cohen, 1987).

Since strains are assumed to be equibiaxial, the in-plane strains ε_{11} and ε_{22} are equal and correspond to an azimuthal angle of 0º. The out-of plane strain, $\varepsilon_{33,}$ corresponds to an azimuthal angle of 90º. The azimuthal angle η^*, at which the radius of the ellipse equals that of the strain-free ring, is independent of stress. The equibiaxial in-plane stress can be calculated using the following equation:

$$\sigma_{11} = \left(\frac{E_{hkl}}{1+\upsilon_{hkl}}\right)\varepsilon_{11}^{hkl} + \frac{\upsilon_{hkl}E_{hkl}}{(1-2\upsilon_{hkl})(1+\upsilon_{hkl})}\left(2\varepsilon_{11}^{hkl} + \varepsilon_{33}^{hkl}\right),$$

where E_{hkl} is the elastic modulus of a specific crystallographic direction and υ_{hkl} is the Poisson's ratio for the hkl crystallographic direction (Noyan and Cohen, 1987).

Since X-ray elastic constants for the ytterbium silicates are not well established in the literature, separate *in-situ* loading experiments on bulk $Yb_2Si_2O_7$ were needed to determine these constants. Plasma-sprayed bulk samples, 8 x 3 x 1 mm^3 parallelepipeds, were compressively loaded to stresses up to 150 MPa and the change in lattice parameters was measured to obtain a stress-strain curve and elastic modulus for the specific crystallographic direction. For the measurements on the bulk samples the beam size was chosen to be 100 x 100 μm^2 to increase the number of grains involved in diffraction and at least five one-second exposures were taken at each point to improve counting statistics. In order to verify that the loading was uniform, measurements were taken and analyzed over the entire width of the sample. The results of these experiments as well as the elastic moduli used for mullite, silicon (Harder et al., 2009a), and silicon carbide (Hellwege, 1979) are summarized in Table 1.

In addition to room temperature measurements, *in-situ* heating experiments were also performed. The $Yb_2Si_2O_7$ EBC samples were heated to and cooled from 1400°C in steps of 200°C in argon inside a resistance furnace (Linkam TS1500 Heating Stage) using beam sizes and translations described for room EBC temperature measurements.

In order to model the stresses in the system, the CTE of the topcoat also had to be established. As the samples are heated, interplanar spacings increase. These increases are very large compared to any strains caused by residual stresses and cause a uniform contraction of the ring, making the effects separable. CTEs were determined for three orthogonal directions and then averaged to provide a bulk CTE value.

Numerical prediction for the residual stresses in the multilayer structure at room temperature were calculated using Multitherm© Ver 1.4 (Finot and Suresh, 1995), a software for thermo-mechanical analysis of multilayered and functionally graded materials. For the numerical predictions, the stress-free state was set to 1200°C, the temperature of the substrate during plasma spraying. The model was then used to predict the stresses as the coating cools down to room temperature. All the relevant mechanical properties used in the model are summarized in Table 1.

Table 1: Summary of the elastic properties of the materials used in this study, (# - determined in this study, * - data from Harder, 2009a, ^ - data from Hellwege, 1979)

Material	Crystallographic Planes (hkl)	Elastic Modulus (GPa)	Poisson's Ratio	CTE ($x10^{-6}$/K)	Function
$Yb_2Si_2O_7$[#]	021	205	0.33	4.7	Environmental Barrier
Mullite[*]	220	145	0.16	5.5	Oxidation Resistant Layer
Silicon[*]	311	187	0.15	4.4	Adhesion Layer
SiC/SiC[^]	220	422	0.17	5.1	Structural Composite

III. RESULTS AND DISCUSSION

SEM micrographs of $Yb_2Si_2O_7$/Mullite/Si/(SiC/SiC) multilayer EBCs are shown in Figure 4. No through-thickness cracking or delamination can be seen in either the as-sprayed (Figure 4a) or the heat-treated sample (Figure 4b). The thicknesses of the intermediate layers vary significantly within the coating and are intrinsic to the plasma spraying process. At some locations the mullite is in direct contact with the SiC/SiC substrate. This has previously been observed in BSAS plasma-sprayed multilayer EBCs (Harder et al., 2009b; Lee et al., 2005).

Residual stress as a function of depth at room temperature of an as-sprayed sample and a sample heat-treated at 1300°C for 100h is shown in Figure 5a and 5b, respectively. In the as-sprayed sample the sample topcoat is under an average compressive stress of 110 MPa, while the topcoat for the heat-treated sample is under a compressive stress of approximately 80 MPa. The average compressive stress in the topcoat agrees well with the prediction from the numerical model. The intermediate layers show almost no stress for all tested $Yb_2Si_2O_7$ EBCs while the numerical model predicts stresses in the mullite and silicon to be 100 MPa and -120 MPa, respectively.

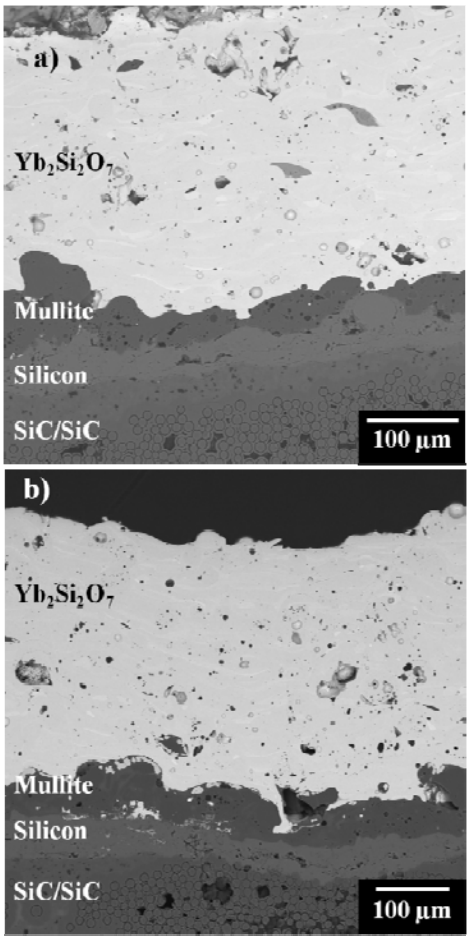

Figure 4. SEM micrographs of $Yb_2Si_2O_7$/Mullite/Si/(SiC/SiC) multilayer EBCs a) as-sprayed and b) heat treated in flowing air at 1300°C for 100h.

Although the reason for the discrepancy with the numerical predictions is unclear, one possible explanation is the uneven and discontinuous nature of the intermediate layers not supporting stresses.

The stresses in the SiC/SiC substrate were measured to a depth of approximately 1 mm into the substrate. They are of the same magnitude as the model (40 MPa at the Si/(SiC/SiC) interface) and decrease deeper into the substrate, as the model predicts. The wavelength of the sinusoidal variations in the stress corresponds to the thickness of the SiC bundle layers that are woven together to form the SiC fiber phase. These sinusoidal variations also exist in an uncoated melt-infiltrated SiC/SiC composite (Figure 6), and vary with the periodicity of the fiber bundle placement (~300-500 μm). It should be noted that the fibers are HI-Nicalon© fibers and have a different SiC stoichiometry, and thus different elastic properties then the melt-infiltrated matrix.

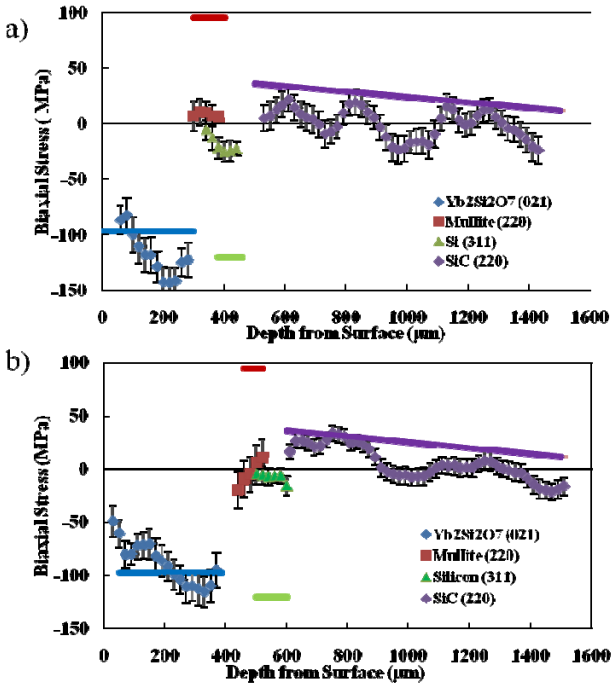

Figure 5. Biaxial stresses as a function of depth in EBC systems with $Yb_2Si_2O_7$ topcoats. a) an as-sprayed sample, b) heat-treated for 100h at 1300°C . Solid lines are numerical predictions.

To gain further insight into the decrease in stress upon the heat-treatment, *in-situ* heating experiments were performed on as-sprayed and heat-treated samples. The results of the *in-situ* experiments are summarized in Figure 7. The magnitude of the initial average compressive stress for the topcoat in the as-sprayed sample is approximately 120 MPa. As the sample is heated the compressive stress in the topcoat decreases, reaching a stress-free state at approximately 1200°C, the temperature at which the coating was deposited. Upon cooling the stress reverts back to compressive but only reaches a magnitude of 70 MPa, a statistically significant decrease from the original state at a confidence level above 95%. This indicates that some relaxation takes place during the first heating cycle. This observation is in agreement with the results from the room-temperature experiments (Figure 5). The relaxation could be caused by several factors. A phase transformation to a less dense phase would decrease compressive stresses. However, no evidence

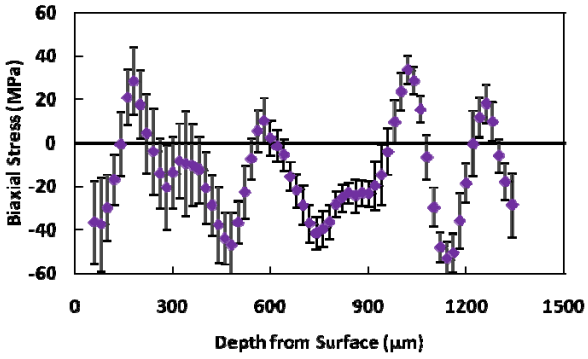

Figure 6. Biaxial stresses as a function of depth in the uncoated, melt-infiltrated SiC/SiC composite for the (220) plane.

for formation of new crystalline phases was found in the diffraction pattern. Voids and preexisting flaws could coalesce and act as nucleating agents for cracks or through thickness cracks could form. No visual confirmation for cracking was found in SEM images both before and after heat treating the EBCs, nor would this be expected given the compressive stress state. A third possibility is the relaxation of quenching stresses which can be relieved on the first thermal cycle (Weyant et al., 2010).

Also in Figure 7, a sample that had been heat treated for 100h at 1300°C has an average compressive stress with a magnitude of 80 MPa at room temperature, within the error of the as-sprayed sample after it has been heated to 1400°C once. When the heat-treated sample is cycled the stress state changes similarly as in the as-sprayed sample but there is no statistically significant difference in stress before and after heating. This shows that once the coating has been heated once, the stress state has stabilized, giving credence to the quenching-stress argument.

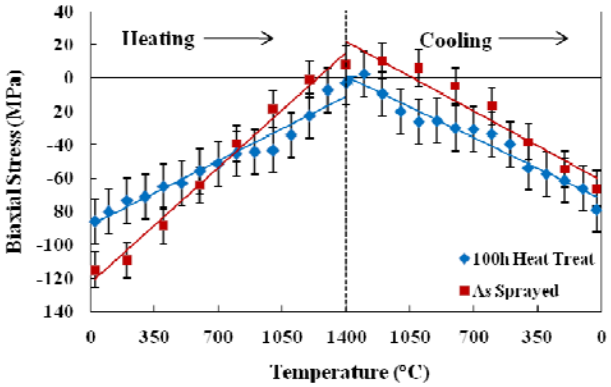

Figure 7. Average biaxial stresses in the (021) direction in the ytterbium disilicate topcoat of a $Yb_2Si_2O_7$/Mullite/Si/(SiC/SiC) EBC as a function of temperature upon heating and cooling, for an as-sprayed sample and a sample heat-treated in air at 1300°C for 100h. Solid lines are least square fits.

This stress state in EBCs with $Yb_2Si_2O_7$ topcoats is conducive to a long operational lifetime. As confirmed by SEM images, residual compressive stresses help to prevent cracking in the coating, thus making for a very effective environmental barrier. The volatility of $Yb_2Si_2O_7$ is comparable to that of BSAS. If the weight loss is constant over time, lifetimes of these coatings and the recession proceeds in a planar fashion, in 50% H_2O-balance O_2 flowing at 4.4 cm/s at 1500° C and 1 atmosphere total pressure, more than 10,000 hours would pass before 10 μm of the topcoat have volatilized.

IV. SUMMARY AND IMPLICATIONS

Residual stresses across multilayer EBCs with $Yb_2Si_2O_7$ topcoats were measured using high-energy X-rays. This technique allows for resolving stresses in EBCs as a function of depth. Elastic constants and the thermal expansion coefficient of the topcoat was also determined using *in-situ* thermo-mechanical loading. The $Yb_2Si_2O_7$ has a lower coefficient of thermal expansion than the mullite layer, resulting in a compressive stress in the topcoat of approximately 100 MPa. On the first heating cycle to 1400°C the magnitude of the compressive stress in the topcoat decreased by approximately 40%, while no change in stress was observed when the same

experiment was performed on a heat-treated sample. The stress relaxation is hypothesized to originate from the relaxation of quenching stresses. The combination of low volatility in combustion environments, a beneficial compressive stress, and no large cracking even after repeated heating to high temperatures make $Yb_2Si_2O_7$ an attractive candidate for an EBC topcoat material.

ACKNOWLDEGEMENTS

Research funding and use of the Advanced Photon Source, an Office of Science User Facility operated for the U.S. Department of Energy (DOE) Office of Science by Argonne National Laboratory, was supported by the U.S. DOE under Contract No. DE-AC02-06CH11357.

REFERENCES

Almer, J., Lienert, U., Peng, R. L., Schlauer, C., and Oden, M. (**2003**).“Strain and texture analysis of coatings using high-energy x-rays,” J. Appl. Phys. **94**, 697–702.

Evans, A. G. and Hutchinson, J. W. (**1984**). “On the mechanics of delamination and spalling in compressed films,” Int. J. Solids Struct. **20**, 455–466.

Faber, K. T., Weyant, C. M., Harder, B. H., Almer, J., and Lee, K. N. (**2007**). “Internal stresses and phase stability in multiphase environmental barrier coatings,” Int. J. Mater. Res. **98**, 1188–95.

Finot, M., Suresh, S. (**1995**). Multitherm, Version 1.4 (Computer Software), MIT, Cambridge, MA.

Harder, B. J., Almer, J. D., Weyant, C. M., Lee, K. N., Faber, K. T. (**2009a**). “Residual Stress Analysis of Multilayer Environmental Barrier Coatings,” J. Am. Ceram. Soc. **92** 452-59.

Harder, B. J., Almer, J.D. Lee, K. N., Faber, K. T. (**2009b**). “*In situ* stress analysis of multilayer environmental barrier coatings” Powder Diff. **24** 94-98.

Hellwege, K. H. (**1979**). *Elastic, Piezoelectric, and Related Constants of Crystals* (Springer-Verlag, Berlin), Vol. 11.

Jacobson, N. S. (**1993**). “Corrosion of silicon-based ceramics in combustion environments,” J. Am. Ceram. Soc. **76**, 3–28.

Lee, K. N. (**2000a**). “Current status of environmental barrier coatings for Si-based ceramics,” Surf. Coat. Technol. **133-134**, 1–7.

Lee, K. N. (**2000b**). "Key durability issues with mullite-based environmental barrier coatings for Si-based ceramics," J. Eng. Gas Turbines Power **122**, 632–636.

Lee, K. N., Fox D. S., Bansal N. P. (**2005**). "Rare earth silicate environmental barrier coatings for SiC/SiC composites and Si_3N_4 ceramics" J. Am. Ceram. Soc. **88** 3483-88.

Lee, K. N., Fox, D. S., Eldridge, J. I., Zhu, D. M., Robinson, R. C., Bansal, N. P., and Miller, R. A. (**2003**). "Upper temperature limit of environmental barrier coatings based on mullite and BSAS," J. Am. Ceram. Soc. **86**, 1299–1306.

Lee, K. N., Miller, R. A., and Jacobson, N. S. (**1995**). "New generation of plasma-sprayed mullite coatings on silicon carbide," J. Am. Ceram. Soc. **78**, 705–710.

Noyan, I. C. and Cohen, J. B. (**1987**) . *Residual Stress: Measurement by Diffraction and Interpretation* (Springer-Verlag, New York).

Opila, E. J. (**1999**). "Variation of the oxidation rate of silicon carbide with water-vapor pressure," J. Am. Ceram. Soc. **82**, 1826–1834.

Opila, E. J., Smialek, J. L., Robinson, R. C., Fox, D. S., and Jacobson, N. S. (**1999**). "SiC recession caused by SiO_2 scale volatility under combustion conditions: II, thermodynamics and gaseous-diffusion model," J. Am. Ceram. Soc. **82**, 1826–1834.

Thouless, M. D. (**1991**). "Cracking and delamination of coatings," J. Vac. Sci. Technol. A **9**, 2510–2515.

Weyant, C. M., Faber, K. T., Almer, J. D., and Guiheen, J. V. (**2005**). "Residual stress and microstructural evolution in tantalum oxide coatings on silicon nitride," J. Am. Ceram. Soc. **88**, 2169–2176.

Weyant, C. M., Faber, K. T., Almer, J. D., and Guiheen, J. V. (**2006**). "Residual stress and microstructural evolution in environmental barrier coatings of tantalum oxide alloyed with aluminum oxide and lanthanum oxide," J. Am. Ceram. Soc. **89**, 971–978.

Weyant, C.M., Almer, J., Faber, K.T. (**2010**). "Through-thickness determination of phase composition and residual stresses in thermal barrier coatings using high energy X-rays," Acta Materialia **58**, 943-957.